JOURNAL OF MATERIALS SCIENCE 15 (1980) 1175–1182

The morphology of α-Fe crystals which grow in the amorphous $Fe_{80}(C_{1-x}B_x)_{20}$ alloys

KIYOSHI SHIMOMURA, PAUL H. SHINGU, RYOHEI OZAKI
Department of Metal Science and Technology, Kyoto University, Yoshida Sakyoku, Kyoto, Japan

Crystallization behaviour of amorphous $Fe_{80}(C_{1-x}, B_x)_{20}$ alloys, obtained by splat-cooling technique, for x values ranging from zero to unity has been investigated mainly by transmission electron microscopy. The crystalline phase which first appeared in the amorphous matrix was α-Fe for all alloys studied. However, the morphology of α-Fe phase changed from a spherical shape for low x values to a watch-glass shape for intermediate x values and to dendritic for large x values. The nucleation of α-Fe crystals was homogeneous for low x samples while preferred nucleation on edges and surfaces was noted for samples with higher x values. The final volume fraction of α-Fe phase before the appearance of the second crystalline phase increased with the increase in x.

1. Introduction

Numerous studies have been performed on the crystallization of amorphous metals concerned mainly with the structure of crystalline phases or the kinetics of crystallization [1–8]. Few studies, however, have been reported on the morphology of crystalline phases which grow in the amorphous matrix, although marked changes in morphology of crystalline phases are often experienced as a result of a small change in the composition of the amorphous alloys. The purpose of this paper is to report the results of a systematic investigation on the morphological change of the crystalline phase which appears from the amorphous $Fe_{80}(C_{1-x}, B_x)_{20}$ alloys by changing x from zero to unity.

2. Experimental details

The gun technique of splat-cooling which is operated in vacuum was employed; details have been reported previously [9]. The heat treatments of samples, vacuum sealed in glass tubes, were performed in a salt bath, the temperature of which was controlled within ± 0.5 K. The X-ray diffractometry of as-splat-cooled samples showed no crystalline peak for the samples with boron content of 10 at % and greater, while for samples with boron content less than 10 at %, crystalline peaks were observed together with the amorphous haloes. Observations by transmission electron microscope (JEM-120) were carried out without applying any thinning treatment. All the electron beam transparent parts of samples were amorphous except for the case of the binary $Fe_{80}C_{20}$ sample which showed co-existing crystalline and amorphous phases in thicker areas.

The position of the 1st halo measured from the electron diffraction film was 3.06 $Å^{-1}$ and hardly any change was observed with the change in boron content while the ratio of the position of 1st and 2nd haloes varied from 1.70 for $Fe_{80}C_{19}B_1$ to 1.66 for $Fe_{80}B_{20}$ samples.

3. Experimental results

3.1. The morphology of the crystalline phase

Fig. 1 shows a series of transmission electron micrographs showing the change in the morphology of the crystalline phase which appears in the amorphous matrix as a result of the change in the relative composition of carbon and boron. The ageings were performed near the crystallization temperatures (temperatures of initiation of crystallization), which are shown in Fig. 2. Although the morphology of these crystals is markedly different for different carbon-to-boron

0022–2461/80/051175–08$02.80/0

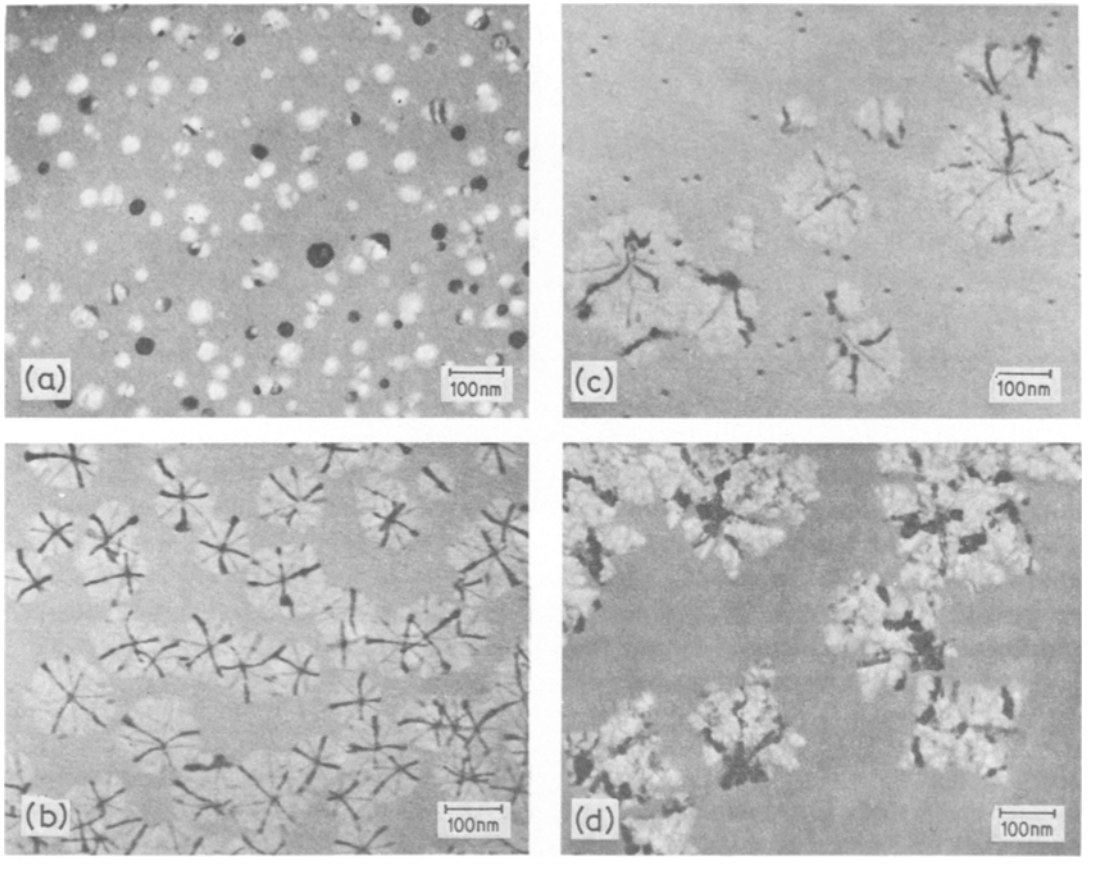

Figure 1 Change in the morphology of α-Fe phase as a result of the change in the carbon to boron ratio: (a) $Fe_{80}C_{19}B_1$, aged at 568 K for 0.9×10^3 sec; (b) $Fe_{80}C_{15}B_5$, aged at 573 K for 1.8×10^3 sec; (c) $Fe_{80}C_{10}B_{10}$, aged at 573 K for 1.8×10^3 sec; (d) $Fe_{80}C_5B_{15}$, aged at 573 K for 57.6×10^3 sec.

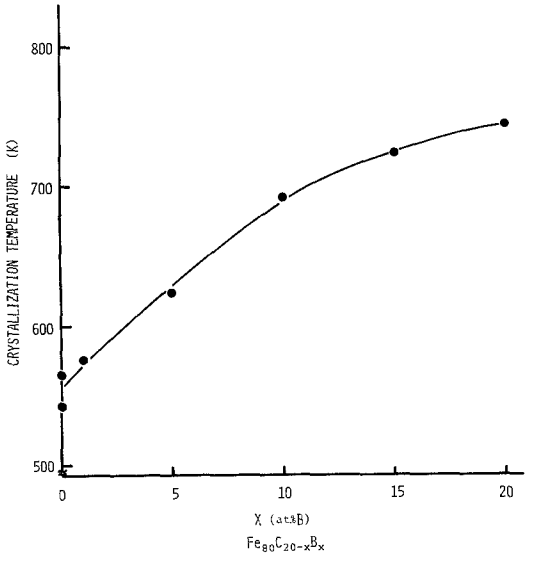

Figure 2 Crystallization temperatures measured by differential scanning calorimetry (DSC) at a heating rate of 5 K min^{-1} as a function of the carbon-to-boron ratio.

ratios, electron diffraction analysis revealed that these crystals are all bcc with the lattice parameter of 2.90 Å, indicating that they are α-Fe [10].

The spherical shape of α-Fe particles shown in Fig. 1a is similar to that for the binary $Fe_{80}C_{20}$ alloy reported previously [9, 11]. While these spherical crystals for high carbon-to-boron ratio, C/B, do not grow to a size beyond several tens of nm in diameter, the reason for which was discussed previously [11], the α-phase for samples of lower C/B grows to over 100 nm diameter and the shape tends to become increasingly irregular and strained as indicated by the appearance of diffraction contrast within each crystalline particle, as shown in Fig. 1b to d.

Fig. 3 shows a series of electron micrographs for samples aged to a later stage of crystallization. For all samples, Fig. 3a to d, at certain stages of growth of α-Fe, the remaining amorphous matrix crystallized into a second crystalline phase dif-

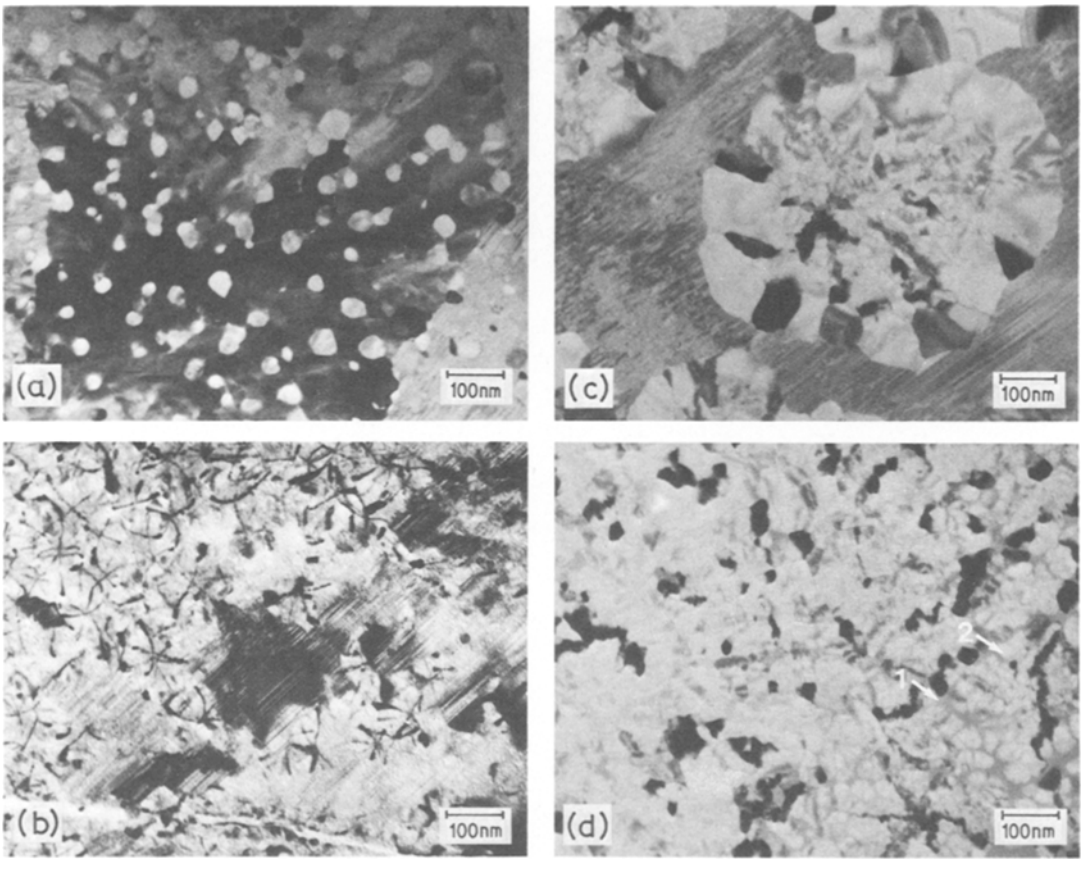

Figure 3 Typical grain structure of samples after the completion of crystallization: (a) $Fe_{80}C_{19}B_1$, aged at 573 K for 1.8×10^3 sec; (b) $Fe_{80}C_{15}B_5$, aged at 573 K for 28.8×10^3 sec; (c) $Fe_{80}C_{10}B_{10}$, aged at 573 K for 28.8×10^3 sec; (d) $Fe_{80}C_5B_{15}$, aged at 573 K for 57.6×10^3 sec.

ferent from the first. The structure of the second crystalline phase for samples a to c in Fig. 3, i.e. for samples with boron content up to 10 at %, was identified as Fe_3C by electron diffraction analysis. The structure of the second phase for samples with boron content more than 15 at % was not identified.

It is to be noted that the amount of the amorphous phase left to crystallize into the second phase becomes smaller as the amount of boron increases relative to that of carbon. The amount of the second phase for the sample of $Fe_{80}C_5B_{15}$ is so small that it can be found only in a narrow channel (indicated by arrow 1 in Fig. 3d) between the impinging α-Fe crystal grains (indicated by arrow 2 in Fig. 3d). The α-phase for samples of lower boron content remained almost unchanged in shape until the start of the formation of the second phase, while in the samples of higher boron content the centre part of the crystalline α-iron particles recrystallized into polycrystals, and a columnar and less-strained α-Fe phase started to grow from it as shown in Fig. 3c.

Fig. 4a to d shows the evidence for the homogeneous nucleation of α-Fe phase in the sample with 1 at % B and the heterogeneous nucleation in samples with 5, 10 and 15 at % B. all the micrographs in Fig. 4 show the part of the sample near the edges. It is to be noted that since the micrographs were taken without applying a thinning treatment, these edge parts are revealed as they were during heat treatment of the samples. No preferential crystallization site is found in Fig. 4a and the distribution of crystalline particles is random, while preferred growth of crystals from edge lines is noted for samples shown in Fig. 4b to d. Growth from an inclusion is also noted in Fig. 4d.

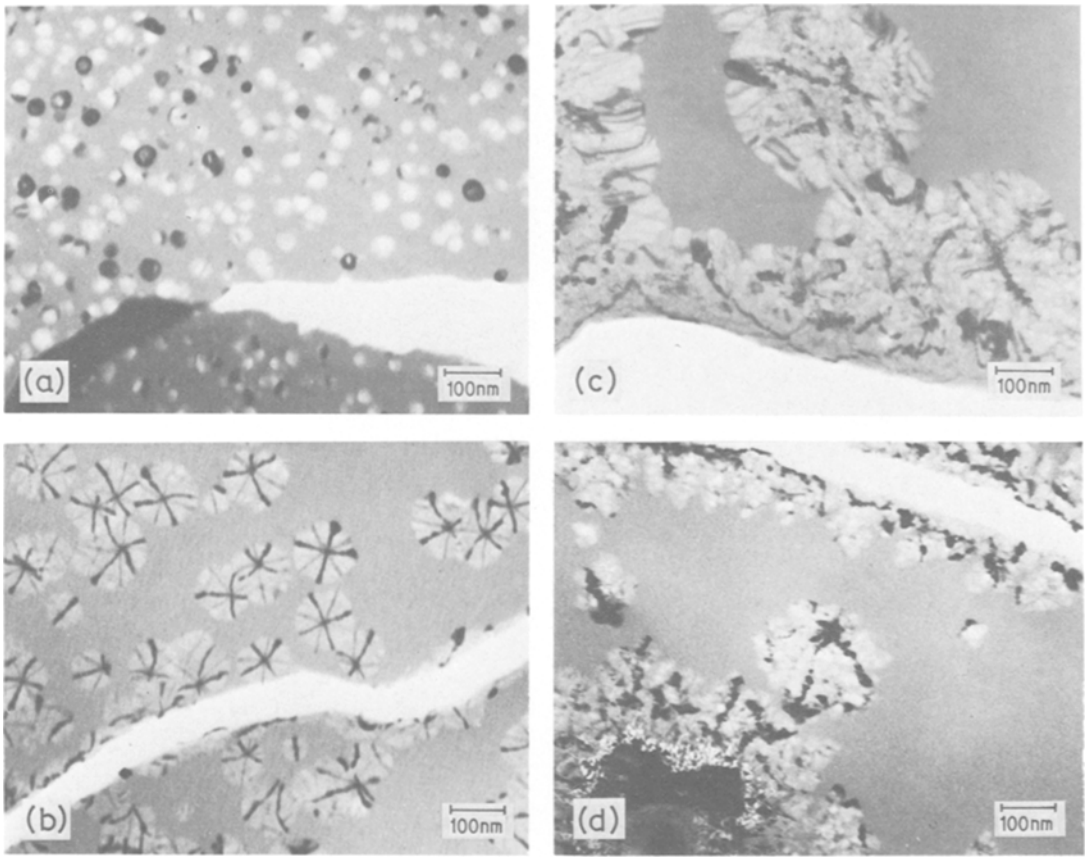

Figure 4 Evidence of homogeneous nucleation for the 1 at.% B sample and heterogeneous nucleation for the 5, 10 and 15 at.% B samples: (a) $Fe_{80}C_{19}B_1$, aged at 568 K for 0.9×10^3 sec; (b) $Fe_{80}C_{15}B_5$, aged at 573 K for 1.8×10^3 sec; (c) $Fe_{80}C_{10}B_{10}$, aged at 573 K for 13.3×10^3 sec; (d) $Fe_{80}C_5B_{15}$, aged at 573 K for 57.6×10^3 sec.

3.2. The diffraction contrast for the $Fe_{80}C_{15}B_5$ sample

The α-Fe phase which appears in the $Fe_{80}C_{15}B_5$ samples is characterized by its regular circular shape and by the distinct cross-shaped diffraction contrasts. Fig. 5a and b shows the corresponding bright- and dark-field images of the α-Fe crystals using a portion of the (1 1 0) diffraction ring. It should be noted that the bright lines in the dark-field image run almost parallel to each other and are nearly perpendicular to the line connecting the incident beam spot and the spot on the (1 1 0) diffraction ring used for the dark-field image, as indicated by the insertion in Fig. 5b. Thus it can be deduced that the circular crystals on the micrographs are bent plates (watch-glass shaped) and that these cross-shaped diffraction contrasts are produced as a result of the bending of the crystals.

A detailed examination by means of an enlarged micrograph of one of the circular crystals, indicated by an arrow in Fig. 5a, is shown in Fig. 6a. The bend contrasts consist of a pair of strong (darker) lines perpendicular to each other and another less strong pair of lines which are also perpendicular to each other. These two pairs of contrast lines are offset by 45° with respect to each other. A closer examination further reveals that each of these contrast lines is composed of two separate lines as indicated in Fig. 6a by the letter *W*. These angular relationships of contrast lines are consistent with the indexing assuming that these are caused as a result of the curvature of the watch-glass shaped thin crystals with their faces parallel to the (0 0 1) plane and lying on the surface of the amorphous sample. The indexing of the contrast lines is given in Fig. 6b. Fig. 6c is a schematic drawing explaining the principle which produces the bend contrast for a watch-glass shaped crystal. The theoretical

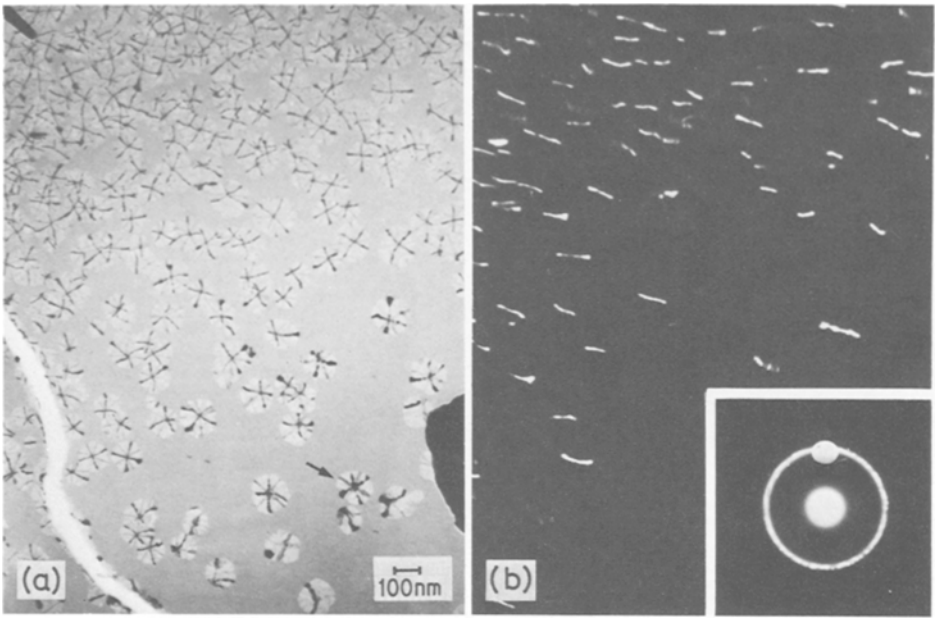

Figure 5 Bright-field image (a) and dark-field image using the (1 1 0) reflection of α-Fe (b) of watch-glass shaped crystals in $Fe_{80}C_{15}B_5$ sample aged at 573 K for 1.8×10^3 sec.

ratio of the diffraction intensity of (1 1 0) and (2 0 0) planes, $I(1\,1\,0)/I(2\,0\,0)$, is nearly 5.0, which supports the indexing given in Fig. 6b.

The radius of curvature of the watch-glass shaped crystal can be calculated by using the simple relation which is readily understood from the schematic drawing given in Fig. 6c,

$$r = Wd/\lambda \qquad (1)$$

where W is the width of the separation of the contrast line as indicated in Fig. 6a to c, d is the spacing of the $(h\,k\,l)$ plane under consideration and λ is the wavelength of the incident electron beam. An example of the calculated values r using the measured value of W for the crystal shown in Fig. 6a is given in Table I. The radius of curvature can also be estimated by the distance of motion of a contrast line due to the inclination of the sample by a known angle, θ, in the electron microscope as explained schematically in Fig. 7a, namely, by the relation

$$r = x/\sin\theta, \qquad (2)$$

where x is the distance of motion of a contrast line. Fig. 7b and c shows electron micrographs of a crystal before and after the inclination of the sample through 6°. The measured distance of motion of the diffraction line is 25 nm which gives a radius of curvature of 240 nm.

4. Discussion

There are three points to be noted about the nucleation and growth of α-Fe crystals from amorphous $Fe_{80}(C_{1-x}, B_x)_{20}$ alloys. These are: (1) the change in morphology of α-Fe crystals with x; (2) the homogeneous nucleation for small x and the heterogeneous nucleation on edges and surfaces for large x samples; and (3) the increase in the ultimate volume fraction of α-Fe phase with the increase in x.

The spherical shape of α-Fe crystals for samples with low x values suggests that the growth anisotropy is suppressed by the large interfacial energy between the crystal and amorphous phases. The fact that no diffraction contrast exists within each spherical crystal indicates that the crystal lattice is not distorted. The crystal–amorphous interface in this case is considered to be incoherent. The watch-glass shaped crystals for samples with 5 or 10 at % boron, on the other hand, are bending in order to keep the coherency at the interface while accommodating the density change due to crystallization. The estimated radius of curvature of around 300 nm gives about a 0.3% linear dimension change due to crystallization, if the thickness of the crystal–amorphous interface is taken to be 1.0 nm. Such a change in length is reported to take place upon crystallization of other amorphous alloys obtained by rapid quenching [12].

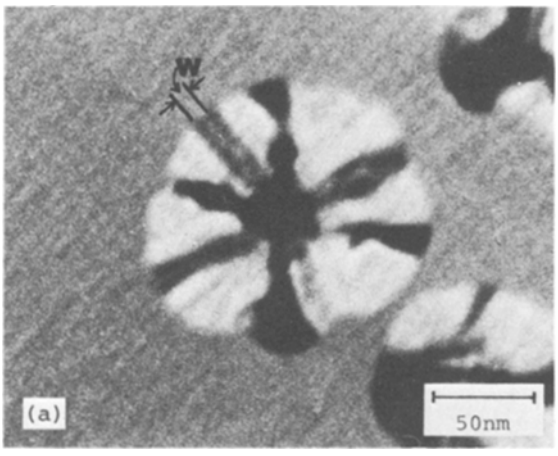

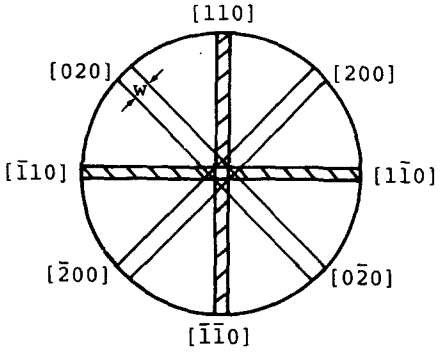

(b) (001) plane

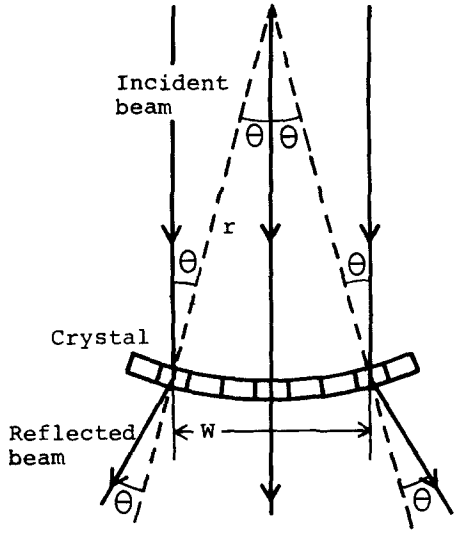

(c)

Figure 6 Explanation of the diffraction contrast in a watch-glass shaped crystal: (a) an enlarged view of a watch-glass shaped crystal shown by an arrow in Fig. 5a; (b) indexing of contrast lines; (c) schematic drawing explaining the origin of contrast lines for the watch-glass shaped crystal.

The change in morphology to dendritic shape for samples of high boron content may be explained as due to the reduction in the interfacial energy owing to the decrease in the density difference between the crystal and amorphous phases. However, factors such as the difference in solubility of boron and carbon in α-Fe or the difference in the diffusivity of these elements in amorphous matrix should also be responsible for the dendritic growth of α-Fe phase.

The heterogeneous nucleation on edges and surfaces for the crystals of higher boron content samples may be explained as due to the coherency between the crystal and amorphous phases, since the strain energy can be reduced by the growth on edges or surfaces when the coherency strain is necessary for nucleation. In the case of low boron content samples, it may be considered that the density change due to crystallization is large, so that the interface becomes incoherent at early stages of crystallization, hence the preference of the nucleation site becomes unnecessary.

TABLE I Result of calculation of the radius of curvature of a watch-glass shaped crystal shown in Fig. 6a

	(1 1 0)	(2 0 0)
d (nm)	0.203	0.143
θ (°)	0.473	0.669
W (nm)	5.0	7.5
r (nm)	300	320
I/I_0	100	19

The ultimate volume fraction of α-Fe phase is larger for samples of higher boron content indicating that a part of total boron in the amorphous phase is incorporated into the crystalline phase to form the solid solution, while carbon is almost totally rejected into the amorphous matrix. The fact that the lattice parameter of α-Fe, estimated by the electron diffraction rings, does not show a noticeable change with increase in boron content, indicates that the change in the lattice parameter due to the solution of boron into α-Fe is small, as reported by Ray and Hasegawa [13].

5. Conclusions

The crystallization process of amorphous $Fe_{80}(C_{1-x}, B_x)_{20}$ alloys was studied by changing the

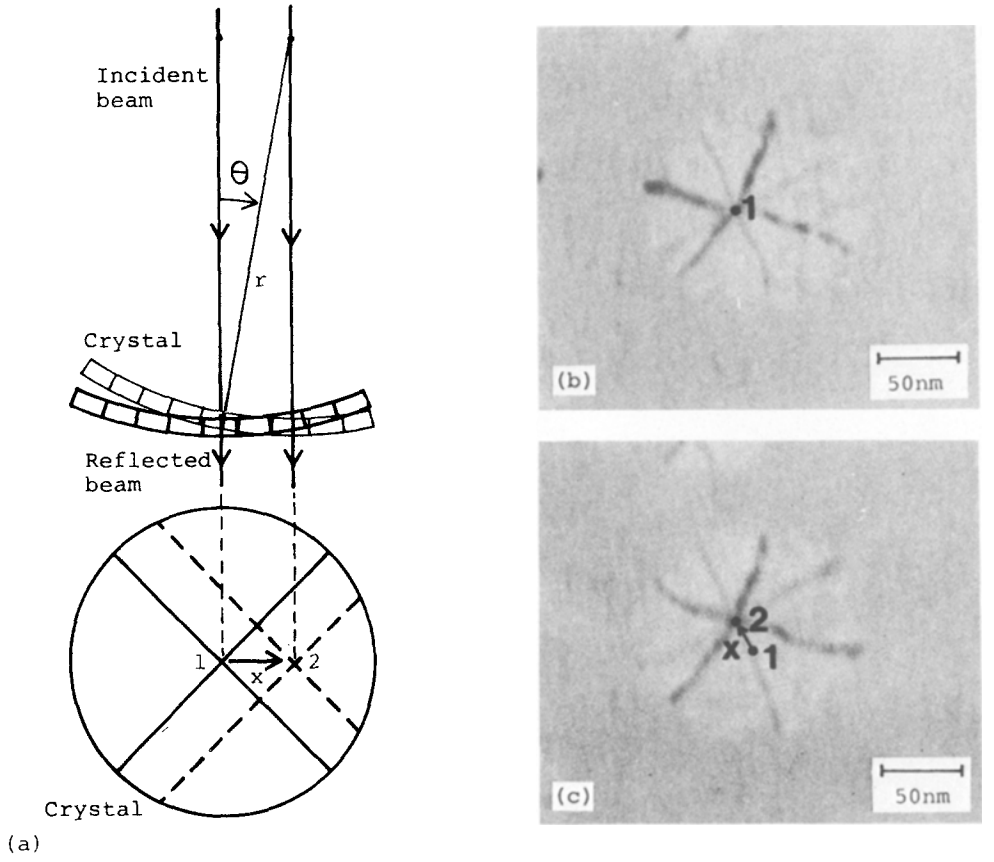

Figure 7 Motion of contrast lines due to the inclination of a sample: (a) schematic drawing explaining the relation between the length of motion and the angle of inclination; (b) before inclination; (c) after inclination by 6°.

x value from zero to unity and the following results were obtained.

(1) The crystallization temperature at a heating rate of 5 K min^{-1} increased from 560 to 750 K corresponding to the increase in x from zero to unity.

(2) By the isothermal ageing near the crystallization temperature, the crystallization proceeds by nucleation and growth of the α-Fe phase for samples of all x values. The appearance of Fe_3C phase was confirmed at a later stage of crystallization for samples with x less than 0.5.

(3) The morphology of the α-Fe phase is spherical for small x values, watch-glass shaped for intermediate x values and dendritic for high x value samples.

(4) The nucleation is homogeneous for small x values while the nucleation on edges and surfaces is noted for samples of higher boron content.

(5) The ultimate volume fraction of α-Fe phase before the appearance of the second crystalline phase increases with the increase in x.

Acknowledgements

The authors wish to thank Dr K. Kobayashi for helpful comments and Mr T. Hori for the assistance in the experiments. This work was supported in part by the Grant in Aid for Scientific Research through the Ministry of Education, Japan.

References

1. M. G. SCOTT, "Rapidly Quenched Metals III", edited by B. Cantor, Vol. 1 (The Metals Society, London, 1978) p. 198.
2. E. HORNBOGEN and I. SCHMIDT, *ibid*, p. 261.
3. U. HEROLD and U. KÖSTER, *ibid*, p. 281.
4. A. L. GREER and J. A. LEAKE, *ibid*, p. 299.
5. J. L. WALTER and S. F. BARTRAM, *ibid*, p. 307.
6. A. S. SCHAAFSMA, H. SNIJDERS and F. VAN DER WOUDE, *ibid*, p. 428.
7. F. E. LUBORSKY, *Mater. Sci. Eng.* 28 (1977) 139.
8. J. L. WALTER, S. F. BARTRAM and R. R. RUSSELL, *Met. Trans. A.* 9A (1978) 803.
9. P. H. SHINGU, K. KOBAYASHI, K. SHIMOMURA and R. OZAKI, *Scripta Met.* 8 (1974) 1317.
10. JCPDS International Centre for Diffraction Data, Powder Diffraction File, No. 6-0696; H. E. SWANSON *et al.*, NBS Circular 539, Vol. IV (1955) p. 3.

11. P. H. SHINGU, K. SHIMOMURA, K. KOBAYASHI and R. OZAKI, *Mater. Sci. Eng.* **23** (1976) 183.
12. P. H. SHINGU, K. SHIMOMURA, R. OZAKI, K. OSAMURA and Y. MURAKAMI, "Rapidly Quenched Metals III", edited by B. Cantor, Vol. 1 (The Metals Society, London, 1978) p. 315.
13. R. RAY and R. HASEGAWA, *Sol. Stat. Commun.* **27** (1978) 471.

Received 21 August and accepted 24 September 1979.